ACS OMEGA

Article

Cite This: ACS Omega 2019, 4, 4604−4614

http://pubs.acs.org/journal/acsodf

Knoevenagel/Tandem Knoevenagel and Michael Adducts of Cyclohexane-1,3-dione and Aryl Aldehydes: Synthesis, DFT Studies, Xanthine Oxidase Inhibitory Potential, and Molecular Modeling

Sahil Arora,[†,§] Gaurav Joshi,[†,§] Sourav Kalra,[†] Aabid Abdullah Wani,[‡] Prasad V. Bharatam,[‡] Pradeep Kumar,[†] and Raj Kumar*[,†]

[†]Department of Pharmaceutical Sciences and Natural Products, Central University of Punjab, Bathinda 151001 Punjab, India

[‡]Department of Medicinal Chemistry, National Institute of Pharmaceutical Education and Research (NIPER), S.A.S. Nagar, Mohali, India

Supporting Information

ABSTRACT: Xanthine oxidase (XO) plays a crucial role in the formation of uric acid by oxidative hydroxylation of purines. Herein, we report the design and synthesis of Knoevenagel/tandem Knoevenagel and Michael adducts of cyclohexane-1,3-dione and aryl aldehydes as nonpurine XO inhibitors derived from naturally occurring scaffolds. Density functional theory calculations highlighted the reaction pathways and reasoned the formation of tandem Knoevenagel and Michael adducts. The synthetics were assessed for their XO inhibitory potential, and among them, four compounds (**1b**, **1g**, **2b**, and **3a**) were found to possess best IC_{50} values in the range of 3.66−4.98 μM. Interestingly, Knoevenagel adducts exhibited a competitive-type inhibition, whereas tandem Knoevenagel and Michael adducts produced a noncompetitive mode of inhibition. The compounds were capable of reducing the H_2O_2 levels induced by XO, both in normal and cancer cells with no significant cytotoxicity. Molecular modeling studies highlighted the role of interactions of compounds with residual amino acids of the XO active site and also corroborated with the observed structure−activity relationship.

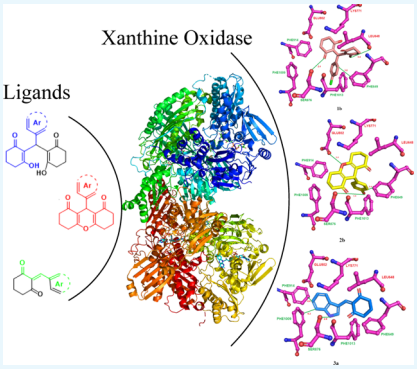

INTRODUCTION

Xanthine oxidase (XO) is a ubiquitous and cytosolic enzyme.[1] It is primarily involved in the purine metabolism and catalyzes the conversion of purines into uric acid via oxidative hydroxylation and uses O_2 as the terminal oxidant of electrons that produces reactive oxygen species (ROS), which upon subsequent reaction with water yields H_2O_2.[2,3] The overexpression of XO elevates the uric acid level, resulting in hyperuricemia and gout, and may also cause other diseases such as metabolic disorder, diabetes,[4] chronic heart failure,[5] hypertension,[6] tissue injury,[7] cancer,[8] inflammation,[9] and oxidative damage.[2,10,11] Inhibition of XO has been found to be beneficial in broad-spectrum therapeutics for above said conditions.[12] Allopurinol was first approved as a XO inhibitor for the treatment of hyperuricemia/gout in 1996. Allopurinol is a purine analogue that inhibits XO reversibly by getting oxidized to oxypurinol.[2] Oxypurinol then binds to a reduced form of XO, that is, [Mo(IV)], via the formation of a covalent bond, thereby exerting its XO inhibitory potential. Eventually, this covalent bond dissociates with time, and XO is reoxidized, re-forming Mo(IV) and leaving behind oxypurinol.[13] The undissociated drug further leads to drug reaction with eosinophilia and systemic symptoms syndrome[14] characterized by skin rash, lymph node enlargement, fever, and single or multiple organ involvement. This occurs due to the inhibition of other purine-utilizing enzymes that include guanine deaminase, hypoxanthine-guanine phosphoribosyltransferase, orotate phosphoribosyltransferase, orotidine-5-monophosphate decarboxylase, and purine nucleoside phosphorylase,[15,16] which is a peculiar feature of purine-based XO inhibitors.[11,17] This led to the quest for selective XO inhibitors derived from nonpurine skeleton, and as a result, febuxostat and topiroxostat (FYX-051) were launched as antihyperuricemic/gout agents in 2009 and 2013, respectively. Although both the agents are exceedingly effective noncompetitive inhibitors of human XO than allopurinol, they are also associated with side effects such as diarrhoea, nausea, headache, arthralgia, rash, and rise in the hepatic serum enzyme level.[18,19] In a recent report, Jordan and Gresser disclosed a cardiovascular-associated death rate due to febuxostat therapy.[20] In addition, febuxostat is currently not used for the treatment of asymptomatic hyperuricemia.[13,21] The newer derivative topiroxostat is more potent than allopurinol and is well-tolerated by patients with renal failures. However, side effects such as elevated alanine aminotransferase decreases the white blood cell count causing eczema nasopharyngitis, and the extreme pain observed with top-

Received: November 2, 2018
Accepted: February 18, 2019
Published: March 1, 2019

DOI: 10.1021/acsomega.8b03060
ACS Omega 2019, 4, 4604−4614

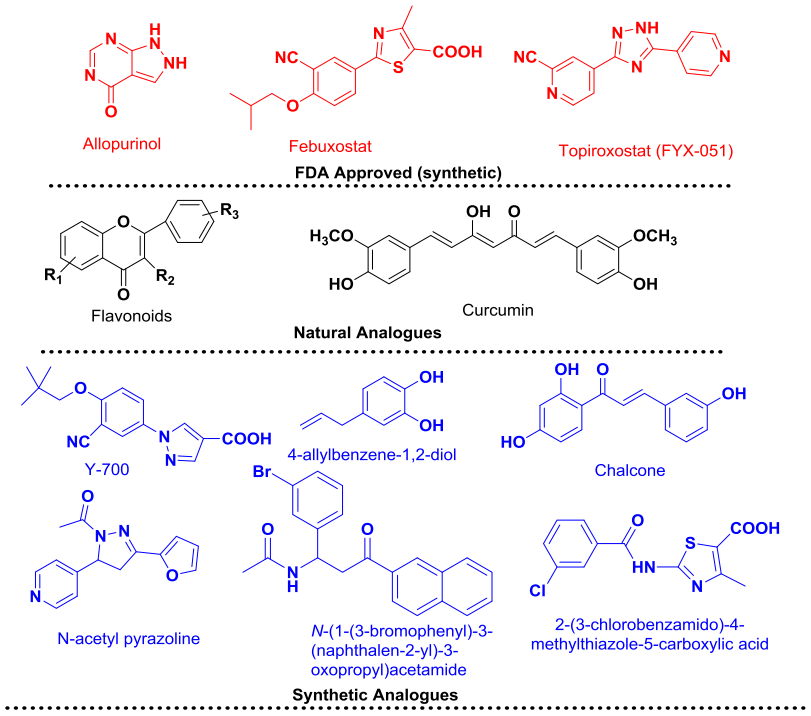

Figure 1. Some reported XO inhibitors.

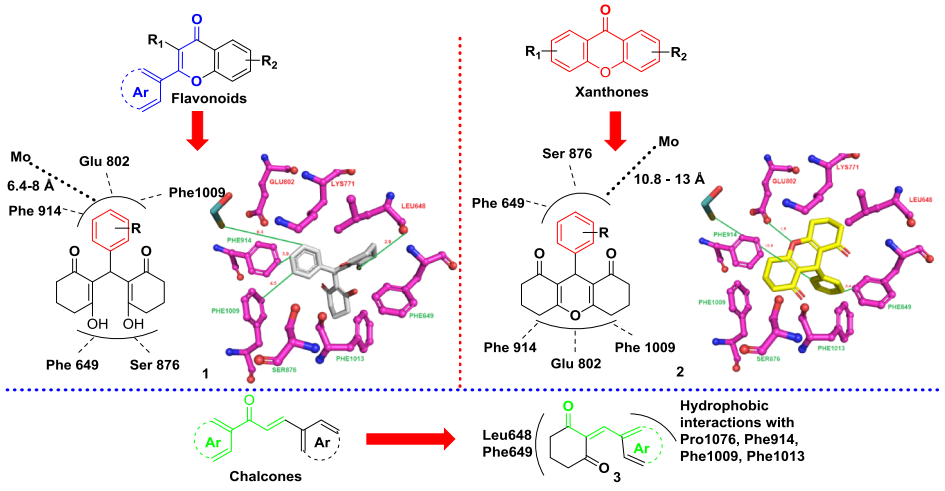

Figure 2. Design strategies for target compounds (**1**, **2**, and **3**) as nonpurine XO inhibitors.

iroxostat in phase 2 trial necessitates the search for new XO inhibitors.[22] Amidst several other classes, chalcones,[23] xanthones,[24] flavonoids,[25] naphthoflavone,[26] azaflavones,[27] pyrazolines/pyrazoles,[28] pyrazoloquinazolines,[29] 2,4-diarylpyrano[3,2-*c*]chromen5(4*H*)-one,[30] and so forth from synthetic or natural origin are reported as XO inhibitors[2,28,29,31] (Figure 1). Considering the toxicities and side effects of both purine as well as nonpurine XO inhibitors, the discovery and development of more potent and selective XO inhibitors devoid of side effects is still warranted.

On the basis of our previous experiences with the discovery of XO inhibitors,[2,28,29,31] we thought of considering easily accessible adducts of 1,3-cyclohexadione and aldehydes (**1**), xanthenes-1,8-diones (**2**), and arylidenes (**3**) as modified nonpurine-based designed leads obtained after scaffold hopping[32−34] of naturally occurring XO inhibitors such as flavonoids, xanthones, and chalcones. In addition, the designed compounds were anticipated to interact with active site amino acid residues of XO more firmly as compared to their parent molecules (Figure 2).

RESULTS AND DISCUSSION

Chemistry. As per the literature reports, the synthesis of target compounds **1**, **2**, and **3** could be accomplished via Knoevenagel[35]/Tandem Knoevenagel and Michael addition of cyclohexane-1,3-dione (**4**) with aryl aldehydes (**5**).[36−47] The Knoevenagel condensation involves use of high boiling solvents dimethylformamide (DMF[48]), acidic or basic ionic liquids ([bmim]Cl·$AlCl_3$, and [bpy]Cl·$AlCl_3$,[36] [bmIm]OH,[40] $[H_3N^+-CH_2-CH_2-OH][CH_3COO-]$,[38] [Hmim]$HSO_4$,[49] [bmim]$BF_4$ with L-histidine[47]), which are difficult to recover, additional organic/inorganic acids or bases [$ZrOCl_2\cdot 8H_2O$ in dry tetrahydrofuran (THF),[42] nano-$ZnAl_2O_4$,[45] taurine (2-aminoethanesulfonic acid)[44] with or without solid support

DOI: 10.1021/acsomega.8b03060
ACS Omega 2019, 4, 4604−4614

(NH_4OAc-basic alumina,[39] $HClO_4$–SiO_2, and PPA–SiO_2,[37]), which require extra treatments during workup and special efforts for the adsorption of the reagents on solid support or need to use special equipment (microwave[39] and ultrasound radiation[50]). Thus, the development of an easy and environmental-friendly synthetic procedure is still required.

Being motivated by the dual activation (electrophilic as well as nucleophilic) role of the solvent[51,52] in the condensation reaction of Meldrum's acid with aryl aldehydes and others, we thought of developing a catalyst-free and environmentally benign methodology for the synthesis of target compounds. To obtain the optimized reaction conditions, a model reaction of cyclohexane-1,3-dione (**4**; 2 equiv) with 4-chlorobenzaldehyde (**5b**; 1 equiv) was carried out at room temperature under catalyst-free condition and in solvents (0.5 mL; Scheme 1)

Scheme 1. Optimization of Reaction Condition for the Synthesis of 1b

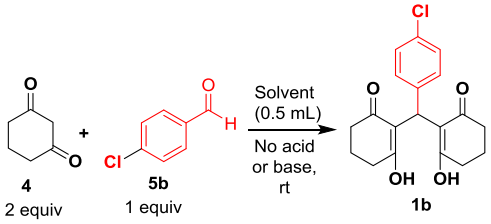

such as PhMe, hexane, $CHCl_3$, DCM, DCE, EtOAc, MeCN, 1,4-dioxane, THF, DMF, dimethyl sulfoxide (DMSO), MeOH, EtOH, ^{i}PrOH, and H_2O. The best results were obtained in carrying out the reaction with methanol as a solvent in 4 h that afforded **1b** (88%) (See Supporting Information, Table S1).

Utilizing the optimized conditions, compounds **1a**–**1h** were synthesized, whereas the target compounds **2a**–**2d** were synthesized by heating the reaction mixture of cyclohexane-1,3-dione (2 equiv) with the corresponding aryl aldehydes (1 equiv) in MeOH. We synthesized one representative compound **3a** to see the effect on XO inhibitory activity (Scheme 2). The compounds were purified by recrystallization from MeOH and characterized by mp, infrared (IR), nuclear magnetic resonance (NMR), and high-resolution mass spectrometry (HRMS).

To rationalize the formation of **1a** via tandem Knoevenagel and Michael addition and the formation of **3a** (not **10**; Scheme 3) as a sole product via Knoevenagel reaction only, quantum chemical studies were carried out to explore the reaction pathways using the B3LYP/6-31+G(d) level. The corresponding potential energy surfaces are plotted in Figures 3 and 4. From Scheme 3 and Figure 3, it is clear that the first step in the reaction requires very comparable activation energies on both the pathways (~28 kcal/mol), however, there are differences in the product stabilities. Product **7** is endothermic (4.46 kcal/mol), whereas product **3a** is exothermic (−0.86 kcal/mol) in comparison to the corresponding starting material. The second C–C bond formation reaction is endothermic on both the pathways (Figure 4). The activation energy for the second step on the pathway leading to **1a** is 29.75 kcal/mol, and the product is 13.6 kcal/mol less stable. The reverse process on this pathway requires 16.15 kcal/mol. The second C–C bond formation reaction along the pathway leading to **10** requires an activation energy of 35.27 kcal/mol, and the product is less stable by 24.27 kcal/mol. The reverse reaction on this path requires only about 11 kcal/mol. Clearly, the second C–C

Scheme 2. Synthesis of Target Compounds

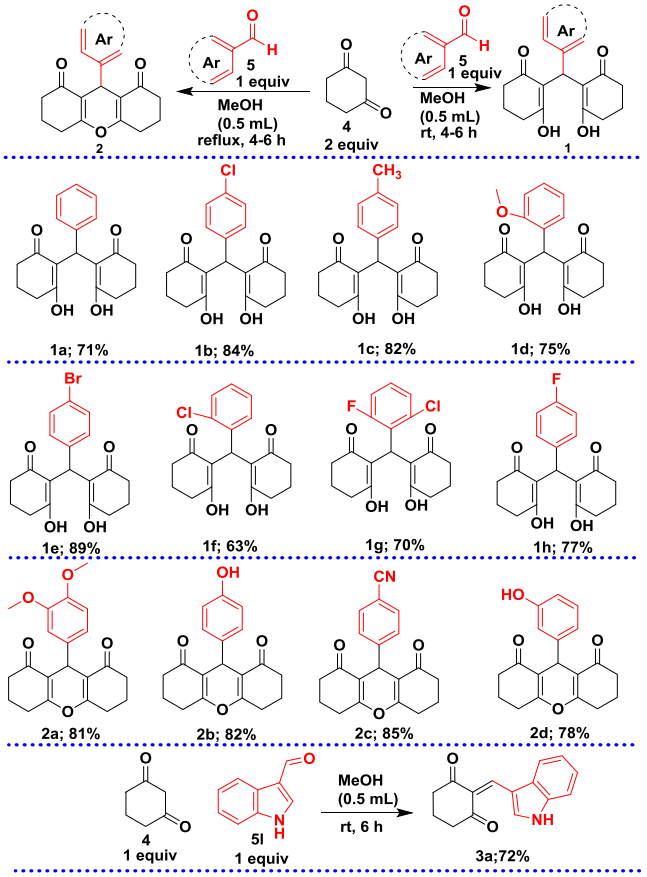

bond formation reaction is energetically more demanding in the case of **10**, thus making this path both thermodynamically and kinetically less favorable. This comparative energy profile analysis explains the absence of product **10** under the experimental conditions along the reaction path as in Scheme 3E.

XO assay[2,28,29,31] is an oxidative enzymatic reaction, which produces uric acid by oxidation of xanthine via utilizing XO. The in vitro XO inhibitory potency of target compounds was determined spectrophotometrically by measuring the uric acid formation at 292 nm. Allopurinol and febuxostat were used as positive controls. The results suggested that **1b**, **1g**, **2b**, **2c**, and **3a** exhibited excellent XO inhibition and reduction in the levels of uric acid (Table 1). To look into the mode of inhibition of XO, Lineweaver–Burke plots of **1g** and **3a** were analyzed. The results suggest that **1g** and **3g** are noncompetitive and competitive-type inhibitors, respectively, as compared to allopurinol that exhibited a competitive mode of inhibition. (Figure 5).

XO is a perilous source of ROS in numerous diseases including inflammatory conditions and cancer.[53] H_2O_2 is a dominant reactive product produced by XO under clinical conditions.[54] To quantify the effect of selected synthetics on H_2O_2 concentration in normal cells, we employed the Amplex Red assay.[55] Chemically, Amplex Red is 10-acetyl-3,7-dihydroxyphenoxazine, a colorless nonfluorescent compound that gets oxidized by H_2O_2 into resorufin in the presence of horseradish peroxidase (HRP).[56] The assay is highly sensitive that may detect as low as 10^{-11} M H_2O_2 in a 100 μL volume. Briefly, we treated embryonic kidney cells (HEK293) with

DOI: 10.1021/acsomega.8b03060
ACS Omega 2019, 4, 4604–4614

Scheme 3. Schematic Representation of the Mechanism for the Formation of 1a and 3a

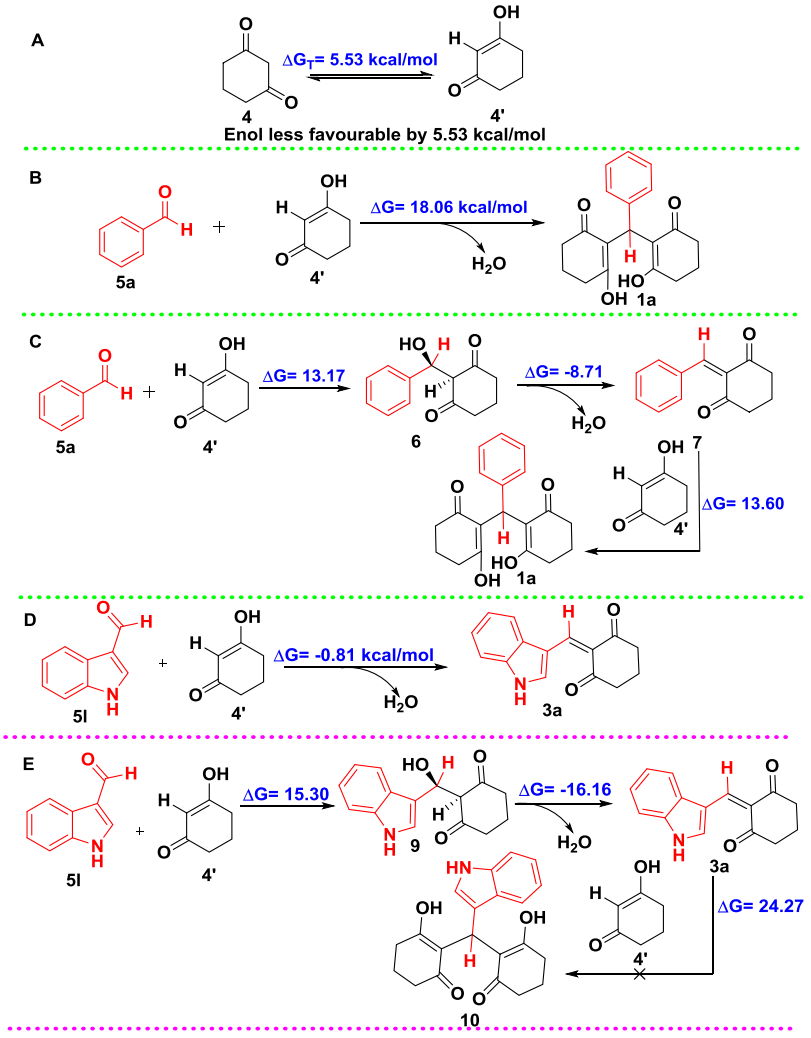

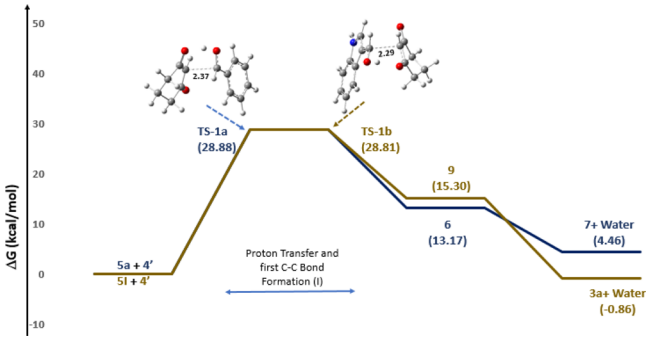

Figure 3. Potential energy surface comparing the energetics of first C−C bond formation products (Scheme 3C−E).

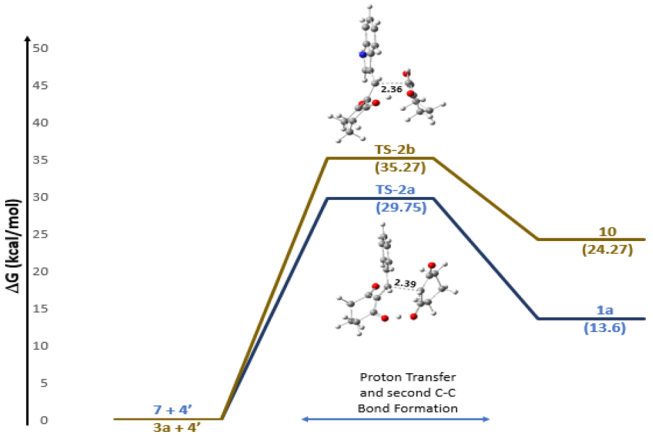

Figure 4. Potential energy surface comparing the energetics of second C−C bond formation products. The compounds inhibited XO and decreased the H_2O_2 levels, with no cytotoxicity toward normal cells.

varying doses of potent XO inhibitors **1b**, **1g**, **2b**, and **3a** (0.5, 1, 5 and 10 μM; Figure 6). The results suggested a dose-dependent decrease in H_2O_2 level that could be due to XO inhibition. As cancer cells produce a high level of H_2O_2, we thought it worthwhile to estimate H_2O_2 levels in cancer cells under the influence of the synthetics. For this, we selected highly invasive and XO-overexpressed MCF-7 (breast cancer) cells.[8] To our delight, synthetics were able to reduce the H_2O_2 levels validating the mechanism that could be via XO inhibition in breast cancer cells. The results were more prominent in MCF-7 than in normal cells (HEK293). Compounds **1b** and **2b** were found to be most potent in terms of reducing the H_2O_2 levels.

Because toxicity is a major issue in drug development,[57,58] we assessed the toxicity (if any) of compounds **1b**, **1g**, **2b**, and **3a** at 10 μM concentrations toward normal cells (HEK293) by

DOI: 10.1021/acsomega.8b03060
ACS Omega 2019, 4, 4604−4614

Table 1. IC_{50} Values of Investigational Compounds

entry	compound code	IC_{50} (μM)[a] ± SD
1	**1a**	15.28 ± 0.28
2	**1b**	4.98 ± 0.55
3	**1c**	13.75 ± 0.31
4	**1d**	9.94 ± 0.49
5	**1e**	10.17 ± 0.39
6	**1f**	9.98 ± 0.61
7	**1g**	4.93 ± 0.53
8	**1h**	5.55 ± 0.79
9	**2a**	5.31 ± 0.81
10	**2b**	4.08 ± 0.67
11	**2c**	5.61 ± 0.77
12	**2d**	13.14 ± 0.45
13	**3a**	3.66 ± 0.57
14	allopurinol	7.08 ± 0.73
15	febuxostat	5.38 ± 0.32[b]

[a]Data are expressed as mean ± standard deviation (SD) of three independent values. [b]Value was obtained as a result of the separate experiment.

the MTT-based assay (Figure 7). The results indicated that no significant cytotoxicity was observed. Thus, the compounds emerged as potential XO inhibitors and were capable of reducing the H_2O_2 levels, both in normal and cancer cells.

Molecular Modeling Study. To investigate the binding of inhibitors with XO, the representative compounds **1b**, **2b**, and **3a** were docked via flexible docking into the active site of XO (PDB: 3bdj)[59] using Glide.[60] All inhibitors were found to occupy the allopurinol binding site. The docking studies revealed that the inhibitors interact mainly with SER876, PHE914, and PHE1009, which are common with most of the known inhibitors (Figure 8).[2] SER876 was involved in the important H-bond interaction with the inhibitors and is found crucial in XO inhibitory activity. Important $\pi-\pi$ interactions were observed between the phenyl ring of the inhibitors and PHE914 and PHE1009. The most active compound **3a** showed the interactions with the important amino acids [SER 876 (H-bond), PHE914, and PHE1009 ($\pi-\pi$ interaction)]. Similarly, for the intermediate active compound **1b**, it was observed that the SER876 interaction was conserved and the H-bond interaction with GLU802 was seen. Further, the docking scores obtained were found to be in accordance with the observed XO inhibitory activity (Table 2).

Nonpurine inhibitors bind to the XO active site at a distance more than 3 Å from the molybdenum center of molybdopterin (MPT) (approximately 5 Å in the case of febuxostat).[2] It was observed that the coordination distances from the molybdenum center to inhibitors **3a**, **1b**, **2b**, and allopurinol were found to be 6.2, 8.0, 6.8, and 2.9 Å, respectively (Figure 9). This study further evidences that synthetics are the nonpurine type of XO inhibitors.

CONCLUSIONS

In summary, we have designed, synthesized, and assessed the in vitro XO inhibitory activity of Knoevenagel/tandem Knoevenagel and Michael adducts of cyclohexane-1,3-dione and aryl aldehydes as nonpurine XO inhibitors. The potent compounds decreased the H_2O_2 levels produced as a result of XO inhibition. Future work will expand the library of compounds based on **3a** and will be published in due course.

EXPERIMENTAL SECTION

Synthesis. *General Procedure for the Synthesis of **1**.* A mixture of 1,3-cyclohexanedione (**4**, 0.20 g, 1.78 mmol, 1 equiv) and aryl aldehyde (**5**, 1 equiv) was dissolved in methanol (0.5 mL), and the reaction mixture was stirred at room temperature for about 4−6 h. The progress of the reaction was monitored by thin-layer chromatography (TLC). After the completion of the reaction (TLC), the precipitate formed was filtered off and washed with excess methanol and dried to afford the crude product. The crude product was further purified by recrystallization from methanol. The remaining reactions were carried out following this general procedure.

Physical data of compounds are given below.

*Synthesis of 2,2′-(Phenylmethylene)bis(3-hydroxycyclohex-2-en-1-one) (**1a**).* Yield: 85%; colorless crystals; mp: 217−219 °C (Lit[44] 219−220 °C); IR (KBr, cm^{-1}): 3388 (OH), 2916 (C−H stretch), 1723 (C═O), 1672 (C═C); HRMS (time-of-flight electrospray ionization (TOF-ESI)): calcd for $C_{19}H_{19}ClO_4$, 312.1362 $[M]^+$; observed, 313.1317 $[M + H]^+$.

*Synthesis of 2,2′-((4-Chlorophenyl)methylene)bis(3-hydroxycyclohex-2-en-1-one) (**1b**).* Yield: 84%; colorless crystals; mp: 199−201 °C; IR (KBr, cm^{-1}): 3483 (OH), 2950 (C−H stretch), 1719 (C═O), 1601 (C═C), 1031−1196 (C−OH stretch), 793 (C−Cl); ^{1}H NMR [$CDCl_3$, 400 MHz, δ (ppm) with trimethylsilane (TMS) = 0]: 12.31 (1H, s), 7.21 (2H, t, J = 8 Hz), 7.01 (2H, s), 5.38(1H, s), 2.60−2.53 (4H, m), 2.39−2.10 (4H, m), 2.00−1.95 (4H, m); ^{13}CNMR ($CDCl_3$, 100 MHz, δ with TMS = 0): 192.39, 191.02, 136.55, 131.65, 128.36, 128.04, 116.26, 33.57, 33.06, 32.62, 20.13; HRMS (TOF-ESI): calcd for $C_{19}H_{19}ClO_4$, 346.0972 $[M]^+$; observed, 347.1127 $[M + H]^+$.

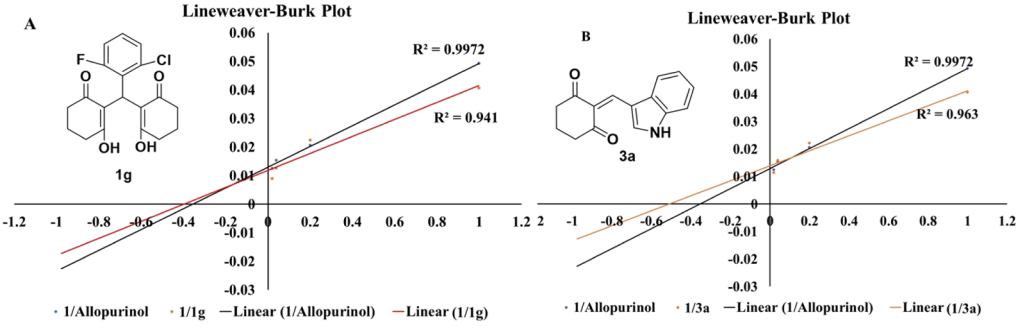

Figure 5. Lineweaver−Burk plots of compounds (A) **1g** and (B) **3a**.

DOI: 10.1021/acsomega.8b03060
ACS Omega 2019, 4, 4604−4614

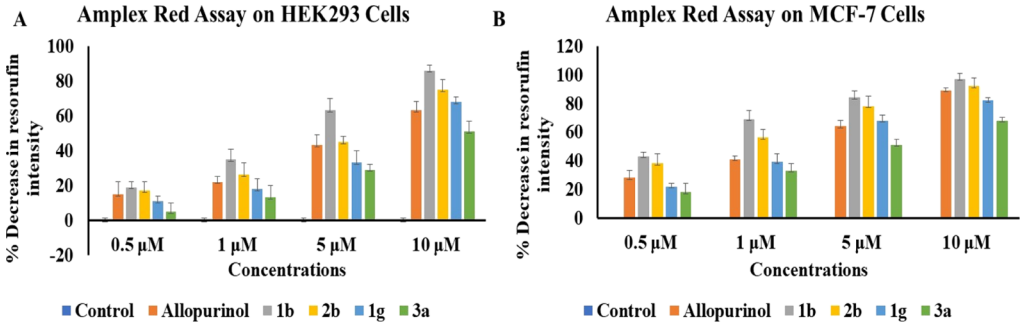

Figure 6. Percentage decrease in resorufin intensity suggesting the reduction in the levels of H_2O_2 upon treatment with **1b**, **1g**, **2b**, and **3a** at a concentration of 0.5, 1, 5, and 10 μM, as indicated by the Amplex Red assay on (**A**) HEK293 cells (**B**) MCF-7 cells.

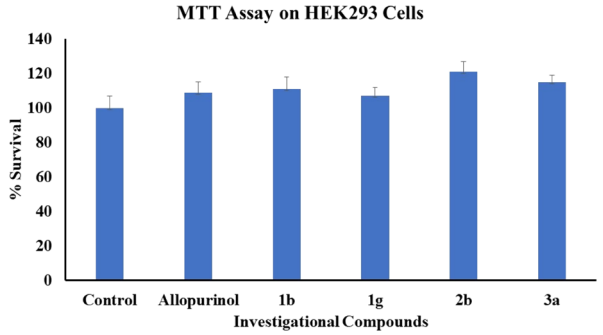

Figure 7. Percentage cell survival (HEK293) after treatment with investigational compounds at a concentration of 10 μM incubated for 24 h.

*Synthesis of 2,2′-(p-Tolylmethylene)bis(3-hydroxycyclohex-2-en-1-one) (**1c**).* Yield: 82%; colorless crystals; mp: 197−199 °C; IR (KBr, cm^{-1}): 3406 (OH), 3170 (OH), 2950 (C−H stretch), 1715 (C═O), 1607 (C═C), 1177 (C−OH stretch); ^{1}H NMR (DMSO-d_6, 400 MHz, δ (ppm) with TMS = 0): 7.01 (2H, d, J = 8 Hz), 6.95 (2H, d, J = 8 Hz), 4.48 (1H, s), 2.60−2.47 (4H, m), 2.22−2.15 (4H, t, J = 4 Hz), 1.98−1.92 (4H, m); ^{13}C NMR (DMSO-d_6, 100 MHz, δ with TMS = 0): 196.29, 165.16, 142.15, 129.02, 128.36, 100.46, 116.13, 36.89, 26.91, 21.04, 20.98; HRMS (TOF-ESI): calcd for $C_{20}H_{22}O_4$, 326.1518 $[M]^+$; observed, 327.1539 $[M + H]^+$.

*Synthesis of 2,2′-((2-Methoxyphenyl)methylene)bis(3-hydroxycyclohex-2en-1-one) (**1d**).* Yield: 75%; colorless crystals; mp: 203−205 °C; IR (KBr, cm^{-1}): 3361 (OH), 3266 (OH), 2949 (−C−H stretch), 1710 (C═O), 1611 (C═C); ^{1}H NMR (DMSO-d_6, 400 MHz, δ (ppm) with TMS = 0): 6.99 (1H, t, J = 8 Hz), 6.81 (1H, s), 6.73 (1H, s), 6.65 (1H, s), 4.49 (1H, s), 3.67 (3H, s), 2.47−2.45 (4H, m), 2.39−2.28 (4H, m), 1.90−1.85 (4H, m); ^{13}C NMR (DMSO-d_6, 100 MHz, δ with TMS = 0): 196.15, 169.85, 156.61, 131.76, 126.84, 120.04, 111.54, 101.67, 56.06, 37.33, 29.07, 21.05, 20.56; HRMS (TOF-ESI): calcd for $C_{20}H_{22}O_5$, 342.1467 $[M]^+$; observed, 343.1490 $[M + H]^+$.

*Synthesis of 2,2′-((4-Bromophenyl)methylene)bis(3-hydroxycyclohex-2-en-1-one) (**1e**).* Yield: 89%; light brown color crystals; mp: 205−207 °C; IR (KBr, cm^{-1}): 3335 (OH),

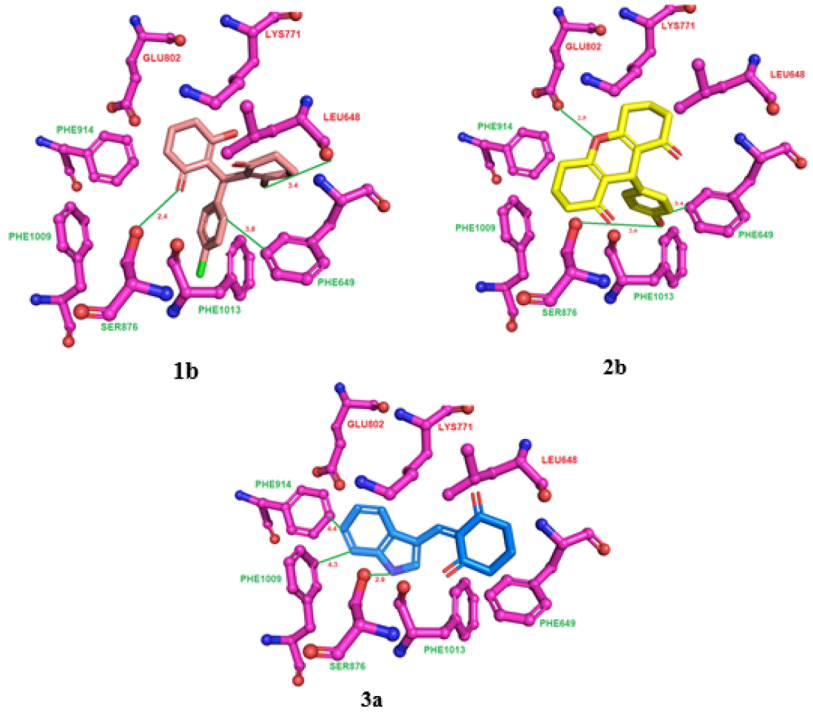

Figure 8. Interaction of the ligands with the important residues at the catalytic XO binding site.

DOI: 10.1021/acsomega.8b03060
ACS Omega 2019, 4, 4604−4614

Table 2. Inhibitors Showing the Interactions with the Important Residues of the Catalytic XO Site[a]

Cd	LEU648	PHE649	GLU802	SER876	PHE914	PHE1009	docking scores	IC_{50} (μM)[b] ± SD
1b	[a]	[a]	–	[a]	–	–	−5.07	4.98 ± 0.55
2b	–	–	[a]	[a]	[a]	[a]	−5.48	4.08 ± 0.67
3a	–	–	–	[a]	[a]	[a]	−6.10	3.66 ± 0.57
A	–	–	[a]	–	[a]	[a]	−4.78	7.08 ± 0.73

[a]+ = interaction; − = no interaction; A = Allopurinol. [b]Data are expressed as mean ± SD of three independent values.

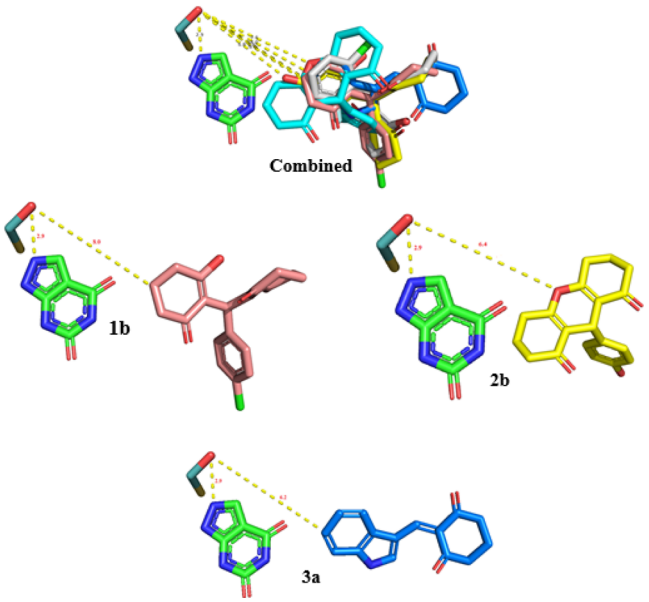

Figure 9. Coordination distances of the synthesized inhibitors (**1b**, **2b**, and **3a**) with the molybdenum center of MPT at the catalytic XO binding site.

2944 (−C−H stretch), 1721 (C═O), 1605 (C═C), 650 (C−Br); ^{1}H NMR ($CDCl_3$, 400 MHz, δ (ppm) with TMS = 0): 12.31 (1H, s), 7.35 (2H, d, J = 8 Hz), 6.95 (2H, d, J = 8 Hz), 5.36 (1H, s), 2.60−2.43 (4H, m), 2.39−2.03 (4H, m), 2.01−1.95 (4H, m); ^{13}C NMR ($CDCl_3$, 100 MHz, δ with TMS = 0): 192.35, 190.95, 137.06, 131.23, 128.37, 119.66, 116.12, 33.49, 33.00, 32.62, 20.06; HRMS (TOF-ESI): calcd for $C_{19}H_{19}BrO_4$, 390.0467 $[M]^+$; observed, 391.0502 $[M + H]^+$.

*Synthesis of 2,2′-((2-Chlorophenyl)methylene)bis(3-hydroxycyclohex-2-en-1-one) (**1f**).* Yield: 63%: colorless crystals; mp: 200−202 °C; IR (KBr, cm^{-1}): 3321 (OH), 2936 (−C−H stretch), 1715 (C═O), 1613 (C═C), 657 (C−Cl); ^{1}H NMR ($CDCl_3$, 400 MHz, δ (ppm) with TMS = 0): 7.26 (1H, d, J = 4 Hz), 7.06 (2H, t, J = 4 Hz), 6.89 (1H, s), 4.59 (1H, s),2.42−2.25 (4H, m), 2.25−2.15 (4H, m), 1.98−1.93 (4H, m); ^{13}C NMR ($CDCl_3$, 100 MHz, δ with TMS = 0): 191.73, 190.86, 130.59, 129.50, 128.12, 126.40, 116.65, 56.27, 37.13, 33.03, 20.26; HRMS (TOF-ESI): calcd for $C_{19}H_{19}ClO_4$: 346.0972 $[M]^+$; observed, 347.0994 $[M + H]^+$.

*Synthesis of 2,2′-((2-Chloro-6-fluorophenyl)methylene)-bis(3-hydroxycyclohex-2-en-1-one) (**1g**).* Yield: 70%; colorless crystals; mp: 197−199 °C; IR (KBr, cm^{-1}): 3361 (OH), 3266 (OH), 2950 (−C−H stretch), 1710 (C═O), 1125 (C−F), 750 (C−Cl); ^{1}H NMR (DMSO-d_6, 400 MHz, δ (ppm) with TMS = 0): 10.59 (1H, s), 7.10 (1H, d, J = 8 Hz), 7.05 (2H, d, J = 8 Hz), 4.93 (1H, s), 2.52−2.48 (4H, m), 2.46−2.24 (4H, m), 1.98−1.93 (4H, m); ^{13}C NMR (DMSO-d_6, 100 MHz, δ with TMS = 0): 197.15, 152.41, 167.32, 133.11, 128.27, 125.31, 123.81, 114.78, 112.34, 37.06, 27.55, 20.82, 20.50; HRMS (TOF-ESI): calcd for $C_{19}H_{18}ClFO_4$, 364.878 $[M]^+$; observed, 367.0659 $[M+2 + H]^+$.

*Synthesis of 2,2′-((4-Fluorophenyl)methylene)bis(3-hydroxycyclohex-2-en-1-one) (**1h**).* Yield: 77%; colorless crystals; mp: 203−205 °C; IR (KBr, cm^{-1}): 3308 (OH), 2962 (−C−H stretch), 1710 (C═O), 1307 (C−F); ^{1}H NMR (DMSO-d_6, 400 MHz, δ (ppm) with TMS = 0): 7.15 (1H, d, J = 4 Hz), 6.90 (1H, s), 6.90−6.86 (3H, m), 5.35 (1H, s), 3.83 (1H, d, J = 4 Hz), 3.30 (3H, s), 2.47−2.45 (4H, m), 2.45−2.38 (4H, m), 2.10−2.05 (4H, m); ^{13}C NMR (DMSO-d_6, 100 MHz, δ with TMS = 0): 206.54, 196.43, 168.10, 130.61, 114.55, 100.53, 60.23, 33.34, 32.37, 20.95, 20.19; HRMS (TOF-ESI): calcd for $C_{19}H_{19}FO_4$, 330.1267 $[M]^+$; observed, 331.1286 $[M + H]^+$.

*Synthesis of 9-(3,4-Dimethoxyphenyl)-3,4,5,6,7,9-hexahydro-1H-xanthene-1,8(2H)-dione (**2a**).* Yield: 81%: colorless crystals; mp: 193−195 °C; IR (KBr, cm^{-1}): 3425 (OH),2928 (C−H stretch), 1664 (C═O), 1601 (C═C), 1130−1171 (C−OH stretch); ^{1}H NMR (DMSO-d_6, 400 MHz, δ (ppm) with TMS = 0): 6.73 (2H, d, J = 8 Hz), 6.61 (1H, s), 4.50 (1H, s), 3.65 (3H, s), 3.63 (3H, s),2.46−2.25 (4H, m), 2.24−2.15 (4H, m), 1.91−1.82 (4H, d, J = 4 Hz); ^{13}C NMR (DMSO-d_6, 100 MHz, δ with TMS = 0): 196.94, 165.21, 148.66, 147.81, 137.69, 120.16, 116.18, 112.84, 112.20, 55.97, 36.99, 30.63, 26.98, 20.45; HRMS (TOF-ESI): calcd for $C_{21}H_{22}O_5$, 354.1467 $[M]^+$; observed, 377.1232 $[M + Na]^+$.

*Synthesis of 9-(4-Hydroxyphenyl)-3,4,5,6,7,9-hexahydro-1H-xanthene-1,8(2H)-dione (**2b**).* Yield: 82%; colorless crystals; mp: 195−197 °C; IR (KBr, cm^{-1}): 3401 (OH), 3279 (OH), 2918 (C−H stretch), 1715 (C═O), 1607 (C═C), 1177(C−OH stretch); ^{1}H NMR (DMSO-d_6,400 MHz, δ (ppm) with TMS = 0): 9.16 (1H, s), 6.95 (2H, d, J = 8 Hz), 6.58 (2H, d, J = 8 Hz), 4.48 (1H, s), 2.33−2.26 (4H, m), 2.25−2.20 (4H, m), 2.09−1.92 (4H, m); ^{13}C NMR (DMSO-d_6, 100 MHz, δ with TMS = 0): 196.81, 164.95, 156.10, 129.32, 116.41, 115.14, 36.92, 30.23, 26.90, 20.37; Anal. Found: C, 73.49; H, 5.96; HRMS (TOF-ESI): calcd for $C_{19}H_{18}O_4$, 310.1205 $[M]^+$; observed, 333.1176 $[M + Na]^+$ and 217.0979 $[M - C_6H_5O]^+$.

*Synthesis of 4-(1,8-Dioxo-2,3,4,5,6,7,8,9-octahydro-1H-xanthen-9-yl)benzonitrile (**2c**).* Yield: 85%; colorless crystals; mp: 205−207 °C; IR (KBr, cm^{-1}): 3406 (OH), 3170 (OH), 2221 (C≡N stretch), 1719 (C═O), 1600 (C═C); ^{1}H NMR (DMSO-d_6, 400 MHz, δ (ppm) with TMS = 0): 7.64 (2H, d, J = 4 Hz), 7.35 (2H, d, J = 4 Hz), 4.56 (1H, s), 2.6−2.47 (4H, m), 2.46−2.22 (4H, m), 1.93−1.81 (4H, m); ^{13}C NMR (DMSO-d_6, 100 MHz, δ with TMS = 0): 196.88, 165.90, 150.47, 132.48, 129.75, 119.36, 114.97, 109.53, 36.79, 32.16, 26.96, 20.29; Anal. Found: C, 75.33; H, 5.43; N, 4.48; HRMS (TOF-ESI): calcd for $C_{20}H_{17}NO_3$, 319.1208 $[M]^+$; observed, 342.1269 $[M + Na]^+$.

*Synthesis of 9-(3-Hydroxyphenyl)-3,4,5,6,7,9-hexahydro-1H-xanthene-1,8(2H)-dione (**2d**).* Yield: 78%; colorless crystals; mp:192−194 °C; IR (KBr, cm^{-1}): 3474 (OH),

DOI: 10.1021/acsomega.8b03060
ACS Omega 2019, 4, 4604−4614

3377 (OH stretch), 3178 (OH), 2955 (−C−H), 1720 (C═O); ^{1}H NMR (DMSO-d_6, 400 MHz, δ (ppm) with TMS = 0): 9.16 (1H, s), 6.92 (2H, d, J = 8 Hz), 6.57 (2H, d, J = 4 Hz), 6.54 (1H, s), 4.47 (1H, s), 2.47−2.42 (4H, m), 2.40−2.24 (4H, m), 1.91−1.81 (4H, m); ^{13}C NMR (DMSO-d_6, 100 MHz, δ with TMS = 0): 196.78, 165.28, 157.49, 146.36, 129.39, 118.99, 115.67, 113.67, 36.97, 31.04, 27.00, 20.40; HRMS (TOF-ESI): calcd for $C_{19}H_{18}O_4$, 310.1205 $[M]^+$; observed, 311.1221 $[M + H]^+$.

*General Procedure for the Synthesis of 2-((1H-indol-3-yl)methylene)cyclohexane-1,3-dione (**3a**).* A mixture of 1,3-cyclohexanedione (**4**, 0.20 g, 1.78 mmol, 1 equiv) and indole-3-carboxaldehyde (**5l**, 0.26 g, 1.78 mmol, 1 equiv) was dissolved in methanol, and the reaction mixture was stirred at room temperature for about 6 h. The progress of the reaction was monitored by TLC. After the completion of reaction (TLC), the precipitate was filtered off, and washing was done with excess methanol and dried to afford the crude product. The crude product was further purified by recrystallization from methanol.

*Synthesis of 2-((1H-indol-3-yl)methylene)cyclohexane-1,3-dione (**3a**).* Yield: 72%; yellowish color crystals; mp: 162−164 °C; IR (KBr, cm^{-1}): 3445 (N−H), 3049−2766 (C═C), 1668 (C═O), 1610 (C═O); ^{1}H NMR (DMSO-d_6, 400 MHz, δ (ppm) with TMS = 0): 9.44 (1H, s), 8.50 (1H, s), 7.85 (1H, t, J = 4 Hz), 7.58 (1H, d, J = 4 Hz), 7.30 (2H, d, J = 4 Hz), 2.64−2.50 (1H, m), 1.98−1.92 (2H, m); ^{13}C NMR (DMSO-d_6, 100 MHz, δ with TMS = 0): 198.32, 197.67, 140.84, 138.90, 137.05, 130.04, 125.89, 124.01, 122.88, 118.20, 113.57, 112.39, 18.58.; HRMS (TOF-ESI): calcd for $C_{15}H_{13}NO_2$, 239.0946 $[M]^+$; observed, 240.1126 $[M + H]^+$.

Biology. *XO Inhibitory Assay.* XO assay relies on the principle of an oxidative enzymatic reaction that produces uric acid via oxidation of xanthine by the catalytic action of XO. The assay was performed in accordance with our previous reported methodologies.[28,29] Briefly, phosphate buffer (pH 7.5, 50 mM) was prepared by using 9.4 mL of (1M) KH_2PO_4 (potassium phosphate monobasic) and 40.6 mL of K_2HPO_4 (potassium phosphate dibasic). They were mixed together, and the volume was made up to 1000 mL with deionized water. Next, xanthine solution (0.10 mM) was prepared by dissolving 15.2 mg of xanthine in 1 mL of NaOH solution to prepare 0.1 (M) xanthine stock solution (1 μL/mL) in deionized water. HCl (1 M) was added to maintain the pH level. XO enzyme solution (0.1−0.2 unit/mL) was made using 1 mg of lyophilized powder of XO enzyme in 1 mL of cold phosphate buffer reagents to prepare a stock solution of 16 U/mL. From the prepared working solution, the stock solution was diluted up to the required volume. Next, the inhibitory effect on XO was measured under aerobic condition spectrophotometrically at 292 nm. The reaction mixture comprises 1.5 mL of 50 mM potassium phosphate buffer (pH 7.4), 1 mL of test sample solution (1,5, 25, and 50 μM) dissolved in biological grade DMSO, and 0.5 mL of freshly prepared XO enzyme solution. The mixture was then preincubated for 15 min at room temperature. Then, 1 mL of substrate solution (0.10 mM of xanthine) was added to the mixture followed by its incubation for 30 min, and then the reaction was stopped by adding 1 mL of 1M HCl. A blank was prepared by replacing xanthine with phosphate buffer, and the absorbance was measured. Readings were taken in triplicate. The percentage inhibition of XO was measured using the formula

$$\% \text{ inhibition} = [(A_c - A_s)/A_c] \times 100$$

where A_c = absorbance of control (sample in absence of XO inhibitors) and A_s = absorbance of treated samples.

IC_{50} was calculated using Graph Prism Software, and Lineweaver−Burk plotting was done using MS Excel.

Culturing and Maintenance of Cells. The cells used in the experiments were purchased from the National Centre for Cell Science, Pune India. The cells were grown in T-25 flasks (corning) culture medium comprising Dulbecco's modified Eagle's medium, fetal bovine serum (10%), and 1× penicillin-streptomycin antibiotic solution. Cell maintenance was done in an incubator under standard conditions of 5% CO_2 and 95% humidity at 37 °C. Once cells became confluent (70−80%), they were split by trypsinization. Both cancer and normal cells were maintained under the abovementioned conditions.

Amplex Red Assay. Amplex Red reagent was purchased from Invitrogen, India and was as per the manufacturer protocol (catalog no. A12214). The assay relies on the principle that nonfluorescent Amplex red gets oxidized to resorufin (highly absorbing and fluorescent pink compound) in the presence of H_2O_2 under HRP-catalyzed reaction.[55] Briefly, normal (HEK293) and breast cancer (MCF-7) cells were seeded in a 96-well plate and treated with investigational compounds at varying concentrations and were further incubated for 24 h. After the stipulated interval, the media was removed and supplemented with phosphate-buffered saline (1× PBS). Thereafter, 50 μL of Amplex Red (Stock: 50 μM) and HRP (0.1 unit/mL) were added to each well and kept in the dark for 30 min. The fluorescence was measured using a microplate reader 530/590 nm (Ex/Em). Standard curves were obtained using predefined volumes of H_2O_2 along with Amplex red and HRP. The experiment was done in triplicate.

MTT Assay. For the MTT assay, approximately 10 000 cells were seeded in each well of 96-well plates. After 24 h, serum starvation was given for 4 h, before replenishing the complete media. After that, treatment of cells with selected compounds at varying concentrations was given, and the cells were incubated for 24 h. After the stipulated time period, the medium was discarded and cells were washed with 1× PBS. Then, MTT dye 10 μL (5 mg/mL stock) was added to each well, and the plate was incubated in the dark for 4 h. The formazan crystals so formed were dissolved in DMSO, and absorbance was measured at 570 nm using a microplate reader. The results were represented graphically in terms of percent survival.[61−64]

Molecular Modeling. The 3D structure of XO (PDB ID: 3BDJ)[59] was retrieved from Protein Data Bank (www.rcsb.org). The predictions of the binding sites were done on the basis of the ligand (oxypurinol) present in the binding cavity using the receptor grid generation module in Maestro 11.4. Structures of the compounds (ligands) were drawn using ChemDraw Professional. The geometries of the compounds were subsequently optimized by OPLS3 force field using LIGPREP module in Schrodinger (2018−3).[60] The ligands were docked at the binding site of XO using the GLIDE module of Schrodinger software.[65] GLIDE uses a Lamarckian genetic algorithm for the generation of different conformations of a ligand. It was used for the ranking of docked conformations of inhibitors. The Glide score comprises the following equation

DOI: 10.1021/acsomega.8b03060
ACS Omega 2019, 4, 4604−4614

$$\text{Glide score} = 0.065 \times E_{\text{vdW}} + 0.130 \times E_{\text{coul}} + E_{\text{lipo}} + E_{\text{Hbond}} + E_{\text{metal}} + E_{\text{buryP}} + E_{\text{rotB}} + E_{\text{site}}$$

Computational Method. Quantum chemical calculations were employed with Gaussian09 suite of programs.[66] Density functional theory was used for the geometry optimizations and frequency calculations for all structures using the B3LYP[67] functional and the 6-311+G(d,p) basis set. The transition states were confirmed to have only one imaginary frequency. The energy values discussed in the manuscript are based on the free energy (ΔG) changes.

■ ASSOCIATED CONTENT

Supporting Information

The Supporting Information is available free of charge on the ACS Publications website at DOI: 10.1021/acsomega.8b03060.

Gibbs free energy calculations and copies of spectra of the products (PDF)

■ AUTHOR INFORMATION

Corresponding Author

*E-mail: raj.khunger@gmail.com, rajcps@cup.ac.in.

ORCID

Gaurav Joshi: 0000-0002-7812-2871

Prasad V. Bharatam: 0000-0002-7064-8561

Raj Kumar: 0000-0001-5113-6627

Author Contributions

§S.A and G.J. have contributed equally.

Notes

The authors declare no competing financial interest.

■ ACKNOWLEDGMENTS

We are thankful to the Vice Chancellor and Dean Academic Affairs for providing the funds to support the present work. The authors thank CIL, CUPB for the data analysis. S.A. thanks Bristol-Myer Squibb (grant no. 34003085), USA for the financial support. G.J. thanks the CSIR, New Delhi (grant no. 05/1051(0011)/2018-EMR-I) for providing SRF.

■ REFERENCES

(1) Fridovich, I.; Handler, P. Xanthine oxidase IV. Participation of iron in internal electron transport. *J Biol Chem* **1958**, *233*, 1581−1585.

(2) Kumar, R.; Joshi, G.; Kler, H.; Kalra, S.; Kaur, M.; Arya, R. Toward an understanding of structural insights of xanthine and aldehyde oxidases: An overview of their inhibitors and role in various diseases. *Med. Res. Rev.* **2018**, *38*, 1073−1125.

(3) Dawson, J.; Walters, M. Uric acid and xanthine oxidase: future therapeutic targets in the prevention of cardiovascular disease? *Br. J. Clin. Pharmacol.* **2006**, *62*, 633−644.

(4) Desco, M.-C.; Asensi, M.; Marquez, R.; Martinez-Valls, J.; Vento, M.; Pallardo, F. V.; Sastre, J.; Vina, J. Xanthine oxidase is involved in free radical production in type 1 diabetes: protection by allopurinol. *Diabetes* **2002**, *51*, 1118−1124.

(5) Leyva, F.; Anker, S. D.; Godsland, I.; Teixeira, M.; Hellewell, P.; Kox, W.; Poole-Wilson, P.; Coats, A. Uric acid in chronic heart failure: a marker of chronic inflammation. *Eur. Heart J.* **1998**, *19*, 1814−1822.

(6) Jankov, R. P.; Kantores, C.; Pan, J.; Belik, J. Contribution of xanthine oxidase-derived superoxide to chronic hypoxic pulmonary hypertension in neonatal rats. *Am. J. Physiol. Lung Cell Mol. Physiol.* **2008**, *294*, L233−L245.

(7) Del, R. M.; Thaw, H.; Björk, J.; Planker, M.; Arfors, K. Free radicals as mediators of tissue injury. *Acta Physiol. Scand., Suppl.* **1980**, *492*, 43−57.

(8) Battelli, M. G.; Polito, L.; Bortolotti, M.; Bolognesi, A. Xanthine oxidoreductase in cancer: more than a differentiation marker. *Cancer Med.* **2016**, *5*, 546−557.

(9) Meneshian, A.; Bulkley, G. B. The physiology of endothelial xanthine oxidase: from urate catabolism to reperfusion injury to inflammatory signal transduction. *Microcirculation* **2002**, *9*, 161−175.

(10) Chung, H. Y.; Baek, B. S.; Song, S. H.; Kim, M. S.; Huh, J. I.; Shim, K. H.; Kim, K. W.; Lee, K. H. Xanthine dehydrogenase/xanthine oxidase and oxidative stress. *Age* **1997**, *20*, 127−140.

(11) Pacher, P.; Nivorozhkin, A.; Szabó, C. Therapeutic effects of xanthine oxidase inhibitors: renaissance half a century after the discovery of allopurinol. *Pharmacol. Rev.* **2006**, *58*, 87−114.

(12) Kumar, R.; Joshi, G.; Kler, H.; Kalra, S.; Kaur, M.; Arya, R. Toward an Understanding of Structural Insights of Xanthine and Aldehyde Oxidases: An Overview of their Inhibitors and Role in Various Diseases. *Med. Res. Rev.* **2018**, *38*, 1073−1125.

(13) Šmelcerović, A.; Tomović, K.; Šmelcerović, Ž.; Petronijević, Ž.; Kocić, G.; Tomašič, T.; Jakopin, Ž.; Anderluh, M. Xanthine oxidase inhibitors beyond allopurinol and febuxostat; an overview and selection of potential leads based on in silico calculated physicochemical properties, predicted pharmacokinetics and toxicity. *Eur. J. Med. Chem.* **2017**, *135*, 491−516.

(14) Cacoub, P.; Musette, P.; Descamps, V.; Meyer, O.; Speirs, C.; Finzi, L.; Roujeau, J. C. The DRESS syndrome: a literature review. *Am. J. Med.* **2011**, *124*, 588−597.

(15) Becker, M. A.; Schumacher, H. R., Jr.; Wortmann, R. L.; MacDonald, P. A.; Eustace, D.; Palo, W. A.; Streit, J.; Joseph-Ridge, N. Febuxostat compared with allopurinol in patients with hyperuricemia and gout. *N. Engl. J. Med.* **2005**, *353*, 2450−2461.

(16) Stockert, A. L.; Stechschulte, M. Allopurinol to febuxostat: How far have we come. *Clin. Med. Insights: Ther.* **2010**, *2*, 927−945.

(17) Borges, F.; Fernandes, E.; Roleira, F. Progress towards the discovery of xanthine oxidase inhibitors. *Curr. Med. Chem.* **2002**, *9*, 195−217.

(18) Chen, C.; Lü, J.-M.; Yao, Q. Hyperuricemia-related diseases and xanthine oxidoreductase (XOR) inhibitors: an overview. *Med. Sci. Monit.* **2016**, *22*, 2501.

(19) Edwards, N. L. Febuxostat: a new treatment for hyperuricaemia in gout. *Rheumatology* **2009**, *48*, ii15−ii19.

(20) Jordan, A.; Gresser, U. Side effects and interactions of the xanthine oxidase inhibitor febuxostat. *Pharmaceuticals* **2018**, *11*, 51.

(21) Naoyuki, K.; Shin, F.; Toshikazu, H.; Tatsuo, H.; Kenjiro, K.; Toshitaka, N.; Takanori, U.; Tetsuya, Y.; Hisashi, Y.; Yuji, M. An allopurinol-controlled, multicenter, randomized, open-label, parallel between-group, comparative study of febuxostat (TMX-67), a non-purine-selective inhibitor of xanthine oxidase, in patients with hyperuricemia including those with gout in Japan: phase 2 exploratory clinical study. *J. Clin. Rheumatol.* **2011**, *17*, S44−S49.

(22) Drug Bank Record Name: Topiroxostat URL.: http://www.drugbank.ca/drugs/DB01685 (accessed on Jan 11, 2019).

(23) Husain, K.; Wai, L. K.; Jamaluddin, F.; Jamal, J. A.; Ummah Abu, N. Xanthine Oxidase Inhibitory Activity of Selected Chalcone Derivatives. *Open Conf. Proc. J.* **2013**, *4*, 286.

(24) Hu, L.; Hu, H.; Wu, W.; Chai, X.; Luo, J.; Wu, Q. Discovery of novel xanthone derivatives as xanthine oxidase inhibitors. *Bioorg. Med. Chem. Lett.* **2011**, *21*, 4013−4015.

(25) Beiler, J. M.; Martin, G. J. The inhibition of xanthine oxidase by flavonoids and related compounds. *J Biol Chem* **1951**, *192*, 831−834.

(26) Singh, H.; Sharma, S.; Ojha, R.; Gupta, M. K.; Nepali, K.; Bedi, P. M. S. Synthesis and evaluation of naphthoflavones as a new class of non purine xanthine oxidase inhibitors. *Bioorg. Med. Chem. Lett.* **2014**, *24*, 4192−4197.

(27) Dhiman, R.; Sharma, S.; Singh, G.; Nepali, K.; Singh Bedi, P. M. Design and Synthesis of Aza-Flavones as a New Class of Xanthine Oxidase Inhibitors. *Arch. Pharm.* **2013**, *346*, 7−16.

DOI: 10.1021/acsomega.8b03060
ACS Omega 2019, 4, 4604−4614

(28) Nepali, K.; Singh, G.; Turan, A.; Agarwal, A.; Sapra, S.; Kumar, R.; Banerjee, U. C.; Verma, P. K.; Satti, N. K.; Gupta, M. K. rational approach for the design and synthesis of 1-acetyl-3, 5-diaryl-4, 5-dihydro (1H) pyrazoles as a new class of potential non-purine xanthine oxidase inhibitors. *Bioorg. Med. Chem.* **2011**, *19*, 1950−1958.
(29) Kumar, D.; Kaur, G.; Negi, A.; Kumar, S.; Singh, S.; Kumar, R. Synthesis and xanthine oxidase inhibitory activity of 5, 6-dihydropyrazolo/pyrazolo [1, 5-c] quinazoline derivatives. *Bioorg. Chem.* **2014**, *57*, 57−64.
(30) Virdi, H. S.; Sharma, S.; Mehndiratta, S.; Bedi, P. M. S.; Nepali, K. Design, synthesis and evaluation of 2, 4-diarylpyrano [3, 2-c] chromen-5 (4H)-one as a new class of non-purine xanthine oxidase inhibitors. *J. Enzyme Inhib. Med. Chem.* **2015**, *30*, 730−736.
(31) Kumar, R.; Darpan; Sharma, S.; Singh, R. Xanthine oxidase inhibitors: a patent survey. *Exp. Opin. Ther. Pat.* **2011**, *21*, 1071−1108.
(32) Schneider, G.; Neidhart, W.; Giller, T.; Schmid, G. "Scaffold-hopping" by topological pharmacophore search: a contribution to virtual screening. *Angew. Chem., Int. Ed. Engl.* **1999**, *38*, 2894−2896.
(33) Schneider, G.; Schneider, P.; Renner, S. Scaffold-hopping: how far can you jump? *QSAR Comb. Sci.* **2006**, *25*, 1162−1171.
(34) Zhao, H. Scaffold selection and scaffold hopping in lead generation: a medicinal chemistry perspective. *Drug Discovery Today* **2007**, *12*, 149−155.
(35) Jones, G. The Knoevenagel Condensation. *Org. React.* **2011**, *15*, 204−599.
(36) Harjani, J. R.; Nara, S. J.; Salunkhe, M. M. Lewis acidic ionic liquids for the synthesis of electrophilic alkenes via the Knoevenagel condensation. *Tetrahedron Lett.* **2002**, *43*, 1127−1130.
(37) Kantevari, S.; Bantu, R.; Nagarapu, L. HClO4−SiO2 and PPA−SiO2 catalyzed efficient one-pot Knoevenagel condensation, Michael addition and cyclo-dehydration of dimedone and aldehydes in acetonitrile, aqueous and solvent free conditions: Scope and limitations. *J. Mol. Catal. A: Chem.* **2007**, *269*, 53−57.
(38) Yue, C.; Mao, A.; Wei, Y.; Lü, M. Knoevenagel condensation reaction catalyzed by task-specific ionic liquid under solvent-free conditions. *Catal. Commun.* **2008**, *9*, 1571−1574.
(39) Balalaie, S.; Nemati, N. Ammonium acetate-basic alumina catalyzed Knoevenagel condensation under microwave irradiation under solvent-free condition. *Synth. Commun.* **2000**, *30*, 869−875.
(40) Ranu, B. C.; Jana, R. Ionic Liquid as Catalyst and Reaction Medium−A Simple, Efficient and Green Procedure for Knoevenagel Condensation of Aliphatic and Aromatic Carbonyl Compounds Using a Task-Specific Basic Ionic Liquid. *Eur. J. Org. Chem.* **2006**, *2006*, 3767−3770.
(41) van Schijndel, J.; Canalle, L. A.; Molendijk, D.; Meuldijk, J. The green Knoevenagel condensation: solvent-free condensation of benzaldehydes. *Green Chem. Lett. Rev.* **2017**, *10*, 404−411.
(42) Poor Heravi, M. R.; Piri, S. Efficient Knoevenagel condensation reactions catalyzed by activated gel zirconium (IV) oxide. *J. Chem.* **2012**, *2013*, 652805.
(43) Rong, L.; Li, X.; Wang, H.; Shi, D.; Tu, S.; Zhuang, Q. Efficient green procedure for the knoevenagel condensation under solvent-free conditions. *Synth. Commun.* **2006**, *36*, 2407−2412.
(44) Shirini, F.; Daneshvar, N. Introduction of taurine (2-aminoethanesulfonic acid) as a green bio-organic catalyst for the promotion of organic reactions under green conditions. *RSC Adv.* **2016**, *6*, 110190−110205.
(45) Mandlimath, T. R.; Umamahesh, B.; Sathiyanarayanan, K. I. Rapid one pot synthesis of xanthene derivatives by an efficient and reusable nano-ZnAl2O4−An insight into a new process. *J. Mol. Catal. A: Chem.* **2014**, *391*, 198−207.
(46) Fallah, A.; Tajbakhsh, M.; Vahedi, H.; Bekhradnia, A. Natural phosphate as an efficient and green catalyst for synthesis of tetraketone and xanthene derivatives. *Res. Chem. Intermed.* **2017**, *43*, 29−43.
(47) Zhang, Y.; Shang, Z. A Green and Novel Method of Synthesizing 2, 2′-Arylmethylene Bis (3-hydroxy-5, 5-dimethylcyclohex-2-enone) Catalyzed by L-Histidine in Ionic Liquid. *Chin. J. Chem.* **2010**, *28*, 1184−1188.
(48) Yoshioka, E.; Kohtani, S.; Miyabe, H. A Multicomponent Coupling Reaction Induced by Insertion of Arynes into the C O Bond of Formamide. *Angew. Chem., Int. Ed. Engl.* **2011**, *50*, 6638−6642.
(49) Kang, H.; Hu, Y.; Huang, H.; Wei, P. Condensation of 1, 3-cyclohexanedione with aromatic aldehydes catalyzed by acidic ionic liquids. *Heterocycl. Commun.* **2008**, *14*, 223−228.
(50) Cravotto, G.; Demetri, A.; Nano, G. M.; Palmisano, G.; Penoni, A.; Tagliapietra, S. The Aldol Reaction under High-Intensity Ultrasound: A Novel Approach to an Old Reaction. *Eur. J. Org. Chem.* **2003**, *2003*, 4438−4444.
(51) Sandhu, H. S.; Sapra, S.; Gupta, M.; Nepali, K.; Gautam, R.; Yadav, S.; Kumar, R.; Jachak, S. M.; Chugh, M.; Gupta, M. K. and biological evaluation of arylidene analogues of Meldrum's acid as a new class of antimalarial and antioxidant agents. *Bioorg. Med. Chem.* **2010**, *18*, 5626−5633.
(52) Dyson, P. J.; Jessop, P. G. Solvent effects in catalysis: rational improvements of catalysts via manipulation of solvent interactions. *Catal. Sci. Technol.* **2016**, *6*, 3302−3316.
(53) Lacy, F.; Gough, D. A.; Schmid-Schönbein, G. W. Role of xanthine oxidase in hydrogen peroxide production. *Free Radical Biol. Med.* **1998**, *25*, 720−727.
(54) Kelley, E. E.; Khoo, N. K. H.; Hundley, N. J.; Malik, U. Z.; Freeman, B. A.; Tarpey, M. M. Hydrogen peroxide is the major oxidant product of xanthine oxidase. *Free Radical Biol. Med.* **2010**, *48*, 493−498.
(55) Rezende, F.; Brandes, R. P.; Schröder, K. Detection of hydrogen peroxide with fluorescent dyes. *Antioxid. Redox Signaling* **2018**, *29*, 585−602.
(56) Dębski, D.; Smulik, R.; Zielonka, J.; Michałowski, B.; Jakubowska, M.; Dębowska, K.; Adamus, J.; Marcinek, A.; Kalyanaraman, B.; Sikora, A. Mechanism of oxidative conversion of Amplex® Red to resorufin: Pulse radiolysis and enzymatic studies. *Free Radical Biol. Med.* **2016**, *95*, 323−332.
(57) Singh, P. K.; Negi, A.; Gupta, P. K.; Chauhan, M.; Kumar, R. Toxicophore exploration as a screening technology for drug design and discovery: techniques, scope and limitations. *Arch. Toxicol.* **2016**, *90*, 1785−1802.
(58) Li, A. P. Accurate prediction of human drug toxicity: a major challenge in drug development. *Chem.-Biol. Interact.* **2004**, *150*, 3−7.
(59) Okamoto, K.; Eger, B. T.; Nishino, T.; Pai, E. F.; Nishino, T. Mechanism of inhibition of xanthine oxidoreductase by allopurinol: crystal structure of reduced bovine milk xanthine oxidoreductase bound with oxipurinol. *Nucleosides, Nucleotides Nucleic Acids* **2008**, *27*, 888−893.
(60) *Schrödinger Release 2018-3*; LigPrep, S., LLC: New York, NY, 2018.
(61) Chauhan, M.; Joshi, G.; Kler, H.; Kashyap, A.; Amrutkar, S. M.; Sharma, P.; Bhilare, K. D.; Chand Banerjee, U.; Singh, S.; Kumar, R. Dual inhibitors of epidermal growth factor receptor and topoisomerase IIα derived from a quinoline scaffold. *RSC Adv.* **2016**, *6*, 77717−77734.
(62) Kaur, G.; Cholia, R. P.; Joshi, G.; Amrutkar, S. M.; Kalra, S.; Mantha, A. K.; Banerjee, U. C.; Kumar, R. Anticancer activity of dihydropyrazolo [1, 5-c] quinazolines against rat C6 glioma cells via inhibition of topoisomerase II. *Arch. Pharm.* **2018**, *351*, 1800023.
(63) Darpan, D.; Joshi, G.; Amrutkar, S. M.; Baviskar, A. T.; Kler, H.; Singh, S.; Banerjee, U. C.; Kumar, R. Synthesis and biological evaluation of new 2, 5-dimethylthiophene/furan based N-acetyl pyrazolines as selective topoisomerase II inhibitors. *RSC Adv.* **2016**, *6*, 14880−14892.
(64) Joshi, G.; Nayyar, H.; Kalra, S.; Sharma, P.; Munshi, A.; Singh, S.; Kumar, R. Pyrimidine containing epidermal growth factor receptor kinase inhibitors: Synthesis and biological evaluation. *Chem. Biol. Drug Des.* **2017**, *90*, 995−1006.
(65) Friesner, R. A.; Banks, J. L.; Murphy, R. B.; Halgren, T. A.; Klicic, J. J.; Mainz, D. T.; Repasky, M. P.; Knoll, E. H.; Shelley, M.; Perry, J. K. : a new approach for rapid, accurate docking and scoring.

DOI: 10.1021/acsomega.8b03060
ACS Omega 2019, 4, 4604−4614

1. Method and assessment of docking accuracy. *J. Med. Chem.* **2004**, *47*, 1739−1749.
(66) Parr, R. G.; Yang, W. *Density-Functional Theory of Atoms and Molecules, Vol. 16 of International Series of Monographs on Chemistry*; Oxford University Press: New York, 1989.
(67) Lee, C.; Yang, W.; Parr, R. G. Density-functional exchange-energy approximation with correct asymptotic behaviour. *Phys. Rev. B: Condens. Matter Mater. Phys.* **1988**, *37*, 785−789.

DOI: 10.1021/acsomega.8b03060
ACS Omega 2019, 4, 4604−4614